Porous Carbon-Supported Gold Nanoparticles for Oxygen Reduction Reaction: Effects of Nanoparticle Size

Likai Wang,[†] Zhenghua Tang,*,[†,‡] Wei Yan,[†] Hongyu Yang,[†] Qiannan Wang,[†] and Shaowei Chen*,[†,§]

[†]New Energy Research Institute, School of Environment and Energy, South China University of Technology, Guangzhou Higher Education Mega Centre, Guangzhou, 510006, China

[‡]Guangdong Provincial Key Laboratory of Atmospheric Environment and Pollution Control, South China University of Technology, Guangzhou Higher Education Mega Centre, Guangzhou, 510006, China

[§]Department of Chemistry and Biochemistry, University of California, 1156 High Street, Santa Cruz, California 95064, United States

Ⓢ *Supporting Information*

ABSTRACT: Porous carbon-supported gold nanoparticles of varied sizes were prepared using thiolate-capped molecular Au_{25}, Au_{38}, and Au_{144} nanoclusters as precursors. The organic capping ligands were removed by pyrolysis at controlled temperatures, resulting in good dispersion of gold nanoparticles within the porous carbons, although the nanoparticle sizes were somewhat larger than those of the respective nanocluster precursors. The resulting nanocomposites displayed apparent activity in the electroreduction of oxygen in alkaline solutions, which increased with decreasing nanoparticle dimensions. Among the series of samples tested, the nanocomposite prepared with Au_{25} nanoclusters displayed the best activity, as manifested by the positive onset potential at +0.95 V vs RHE, remarkable sustainable stability, and high numbers of electron transfer at (3.60−3.92) at potentials from +0.50 to +0.80 V. The performance is comparable to that of commercial 20 wt % Pt/C. The results demonstrated the unique feasibility of porous carbon-supported gold nanoparticles as high-efficiency ORR catalysts.

KEYWORDS: *porous carbon, gold nanoparticle, size effect, pyrolysis, oxygen reduction*
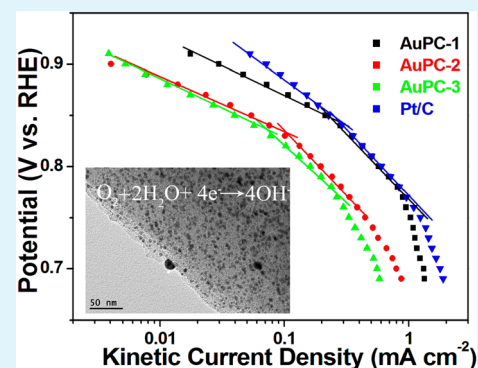
INTRODUCTION

In recent decades, the increasing consumption and rapid depletion of fossil fuels has significantly intensified efforts in search of alternative technologies for efficient energy conversion and storage.[1,2] Of these, fuel cells represent a unique technology where chemical energy is converted into electrical energy by redox reactions at the electrodes. The oxygen reduction reaction (ORR) at the cathode is a critical process that has been known to play a major role limiting the fuel cell efficiency. This is owing to its complex reaction pathways and slow electron-transfer kinetics. Platinum group metals and their alloys have been the leading candidates for ORR catalyst design; yet, the high costs, low stability, as well as limited supply of platinum significantly hinder their large scale commercialization.[3−6] Therefore, significant research efforts have been dedicated to developing platinum-free ORR catalysts by multiple research groups continuously in the past decades.[7−12]

Among these, bulk gold has been observed to exhibit moderate activity in alkaline solutions,[13,14] and significant research efforts have been devoted to developing gold nanoparticles-based hybrid materials for ORR.[15−17] For instance, Erikson et al. examined the ORR activity of carbon supported gold catalysts, and found that the activity varied with

the Au nanoparticle size and catalyst loading.[13] Gold−polyanline nanocomposites have also been fabricated through a facile interfacial polymerization approach by the Vodnik group and exhibited an excellent electrocatalytic capability showing onset potential at −0.1 V vs SCE.[18] As ORR activity is sensitive to the catalyst surface chemistry, the geometric and electronic structure of the gold nanoparticles (NPs) hold an important impact on the catalyst performance. Xu and co-workers found that the ORR activity might be strongly correlated with the Au NPs with the size ranging from 3 to 10 nm, and the size difference had no influence on the mechanism.[19] Tang et al. observed that the kinetic current of 3 nm Au NPs was 3.5 times of 7 nm Au NPs, and the former one took a four electron reduction pathway but the latter one took a two electron reduction pathway.[20] The Kobayashi group investigated the Au nanoparticle size effects on ORR in acidic media, and observed a highest number of electron transfer when the nanoparticles were less than 3 nm in diameter.[21] Lee et al.[22] reported enhanced ORR activity was observed when 8 nm gold nanoparticles were capped with easily removable

oleylamine ligands, as compared with 3 or 6 nm Au nanoparticles passivated by hexadecanethiol. In spite of the progress, most of these prior studies focused on Au NPs larger than 2 nm. Examples have been rare for ultrasmall gold clusters (core diameter <2 nm) for ORR. Notably, drastically enhanced performance has been observed with (sub)nanometer-sized gold clusters (AuNCs). It can be ascribed to the under-coordinated surface atoms that facilitated oxygen adsorption on the nanoparticle surface.[23] In fact, molecular AuNCs (Au_{11}, Au_{25}, Au_{55}, and Au_{140}) have shown apparent ORR activity, which increases with shrinking core size.[23] However, the organic capping ligands may block the availability of catalytic sites on the surface, which significantly limit their catalytical activity.[24] In addition, because of the well-known Ostwald ripening effect,[20] AuNCs may aggregate/grow into larger particles when they are used alone in electrochemical reactions. One effective procedure to mitigate these issues is to remove the organic capping ligands by pyrolysis at controlled temperatures and support the nanoparticles on an appropriate substrate, for instance, graphene,[25] TiO_2,[26] as well as other inorganic materials.[27]

In the present study, using thiolate-capped Au_{25}, Au_{38}, and Au_{144} nanoclusters as precursors, we prepared a series of porous carbon-supported gold nanoparticles. The organic capping ligands were removed by pyrolysis at controlled temperatures, and uniform gold nanoparticles were rather well dispersed within the porous carbon scaffold without obvious agglomeration. These supported gold nanoparticles exhibited excellent electrocatalytic activity for ORR, which increased with diminishing nanoparticle size. Among the nanocomposites tested, the sample derived from Au_{25} nanoclusters showed the best activity and was comparable to commercial 20 wt % Pt/C.

■ EXPERIMENTAL SECTION

Chemicals. Acetone, tetrahydrofuran, dichloromethane, toluene, hydrofluoric acid, and sucrose were purchased from Caiyunfei Chemical Reagents (Tianjin, China). Reduced L-glutathione, hydrogen tetrachloroaurate(III) trihydrate ($HAuCl_4\cdot3H_2O$), tetra-n-octylammonium bromide (TOABr), and 2-phenylethanethiol (HSC_2H_4Ph) were acquired from Energy Chemicals (Shanghai, China). Sodium borohydride ($NaBH_4$) and SBA-15 amorphous silica were obtained from Aladdin Industrial Corporation (Shanghai, China). Commercial 20 wt % Pt/C was purchased from Alfa Aesar. The resistivity of deionized water used in this study was 18.3 MΩ·cm.

Preparation of Gold Nanoparticles Supported by Porous Carbon. Porous carbon (Figures S1−S2)[28] and molecular gold nanoclusters, $Au_{25}(SC_2H_4Ph)_{18}$,[29] $Au_{38}(SC_2H_4Ph)_{24}$,[30] and $Au_{144}(SC_2H_4Ph)_{60}$[31] (abbreviated as Au_{25}, Au_{38}, and Au_{144}) were synthesized by adopting well-established synthetic procedures in the literature (see details in the Supporting Information). The synthesis of porous carbon-supported Au_{25} nanoclusters was described as follows. In a typical reaction, 14 mg of porous carbon was first dispersed into 100 mL CH_2Cl_2. Separately, a solution containing 9 mg of $Au_{25}(SC_2H_4Ph)_{18}$ nanoclusters in 40 mL CH_2Cl_2 was prepared under magnetic stirring for 20 min (corresponding to a gold mass of ca. 6 mg). Then the CH_2Cl_2 solution of Au_{25} was dropwisely added into the above porous carbon dispersion at constant stirring and sonication at ambient temperature for 1 h. After CH_2Cl_2 was removed by rotary evaporation, the precursor underwent pyrolysis at 500 °C for 2 h under a flow of nitrogen, forming nanocomposites where gold nanoparticles were supported on porous carbon at a gold mass loading of 30%. This sample was referred to as AuPC-1. The samples of AuPC-2 and AuPC-3 were fabricated in a similar manner by employing $Au_{38}(SC_2H_4Ph)_{24}$ and $Au_{144}(SC_2H_4Ph)_{60}$ clusters as the respective precursor.

Characterizations. Powder X-ray diffraction (XRD) spectra were acquired by a Bruker D8 diffractometer with Cu Kα radiation (λ = 0.1541 nm). The surface chemical compositions and valence states were examined by X-ray photoelectron spectroscopy (XPS, Phi X-tool instrument). UV−visible absorption spectra of AuNCs were recorded on a Shimadzu 2600/2700 spectrophotometer. TEM analysis of the samples were carried out by a high-resolution transmission electron microscope (JEOL TEM-2010). The metal-to-organic ratio of the Au clusters was determined by thermogravimetry analysis (TGA) with a METTLER instrument under a N_2 atmosphere.

Electrochemistry. All the electrochemical studies were operated on a CHI 750E electrochemical workstation (CH Instruments Inc.) with a conventional three-electrode system at room temperature. The as-prepared catalyst-coated glassy carbon electrode (GCE) was used as the working electrode, and a AgCl/Ag with saturated KCl and a Pt wire were used as the reference electrode and counter electrode, respectively. Prior to catalyst deposition, the GCE was subjected to mechanical polishing with 0.3 um alumina powders on a polishing microcloth. All catalyst inks were fabricated in a same protocol as follows: First, 2 mg of the catalysts prepared above was dispersed into 1.0 mL ethanol containing 10 μL Nafion (5 wt %), then the dispersion was sonicated for 30 min to prepare a homogeneous catalyst ink. The glassy carbon disk was coated with the catalyst ink (10 μL), and the loadings were controlled at 80.8 μg cm^{-2}. Linear sweep voltammograms were collected at the scan rate of 10 mV s^{-1} and cyclic voltammoetric measurements were performed at the scan rate of 10 mV s^{-1}. The durability and stability of the nanocomposite catalysts were examined by chronoamperometric measurements in the O_2-saturated 0.1 M KOH solution at the rotation rate of 900 rpm and the potential of +0.5 V (vs RHE) for 30 000 s. A reversible hydrogen electrode was employed to calibrate the Ag/AgCl reference electrode, and in 0.1 M KOH, $E_{RHE} = E_{Ag/AgCl} + 0.966$ V.

■ RESULTS AND DISCUSSION

The structures of the as-produced $Au_{25}(SC_2H_4Ph)_{18}$, $Au_{38}(SC_2H_4Ph)_{24}$, and $Au_{144}(SC_2H_4Ph)_{60}$ clusters were first characterized, which were found to be consistent with literature results, as manifested in Figures S3−S5.[32,33] The nanoclusters were then loaded onto porous carbons, and the organic capping ligands were removed by calcination, leading to the deposition of gold nanoparticles on the carbon scaffolds. Typical TEM images of the resulting nanocomposite: (A) AuPC-1, (C) AuPC-2, and (E) AuPC-3 are shown in Figure 1. One can see that after calcination, the gold nanoparticles were dispersed rather homogeneously within the carbon substrates (evidenced by the low contrast background), with no obvious agglomeration. The average diameters of Au NPs were estimated to be 3.7 ± 0.90 nm for AuPC-1, 4.9 ± 1.10 nm for AuPC-2, and 5.8 ± 1.25 nm for AuPC-3, as illustrated in the corresponding core size histograms in panels (B), (D), and (F). These are somewhat larger than those of the original gold nanoclusters (Figure S3).

The structures of the AuPC-1, AuPC-2, and AuPC-3 nanocomposites, along with porous carbon alone, were then studied by XRD measurements. From Figure 2, it can be seen that the porous carbon sample exhibited two peaks at 2θ = 23.8 and 43.0° from hexagonal carbon (JCPDS no. 75−1621), consistent with the (002) and (101) crystalline planes, respectively. For the three AuPC nanocomposites, four well-defined peaks can be observed at 38.1°, 44.3°, 64.5°, and 77.4°, which may be attributed to the peak corresponding to the (111), (200), (220), and (311) crystalline planes of *fcc* gold (JCPDS no. 65−2870). Note that the Au(200) facets overlapped with the C(101) peak, whereas the C(002) diffraction appeared to red-shift to about 30°, suggesting lattice contraction due to nanoparticle deposition. These results
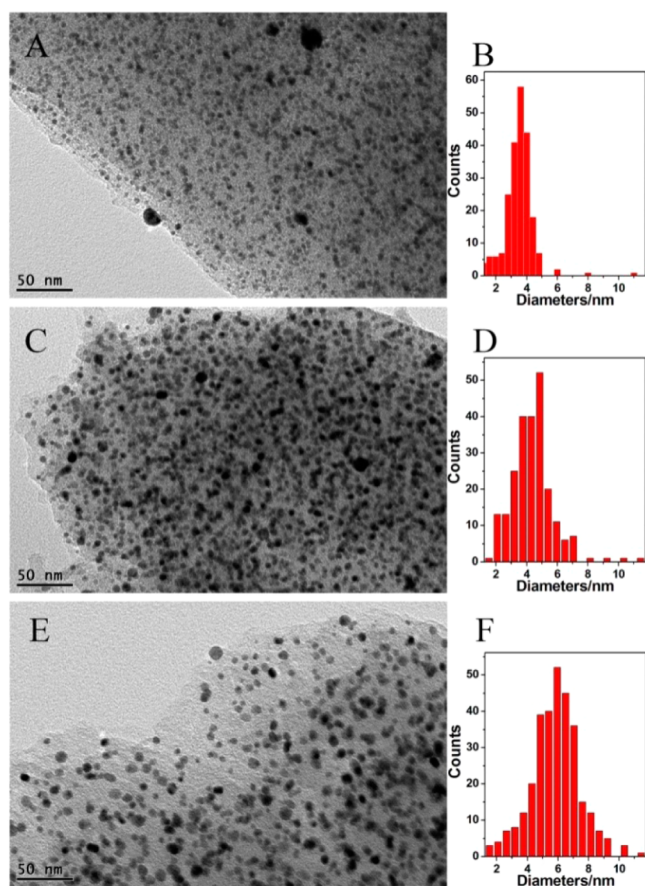
Figure 1. Typical TEM images of (A) AuPC-1, (C) AuPC-2, and (E) AuPC-3, with the corresponding size histograms in panels (B), (D), and (F).
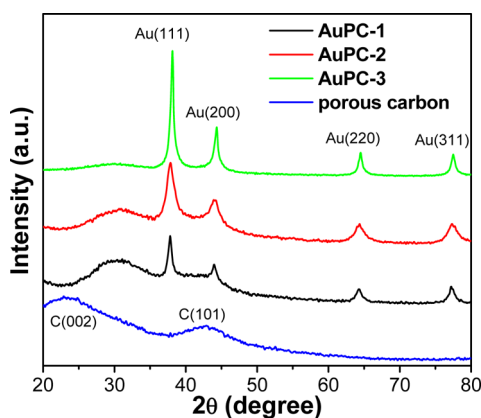

Figure 2. XRD patterns of porous carbon, AuPC-1, AuPC-2, and AuPC-3.

Figure 3. Focus scanning XPS spectra of the (A) C 1s electrons of porous carbon and AuPC-1, and (B) Au 4f electrons of Au_{25} NCs and AuPC-1.

confirmed the successful incorporation of gold nanoparticles into the porous carbon (Figure 1).

Consistent results were obtained in XPS measurements. As demonstrated in Figure S6, the XPS survey spectra confirmed the presence of Au, C, and O elements in the AuPC nanocomposites. Further structural insights were revealed in the high-resolution spectra of the C 1s (Figure 3A) and Au 4f (Figure 3B) electrons. From Figure 3A, one can see that in the AuPC-1 sample, deconvolution of the C 1s spectrum yields three peaks, sp^2 C (284.8 eV), C in C−O (285.9 eV) and C in C=O/COOH (288.0 eV); similar behaviors can be observed
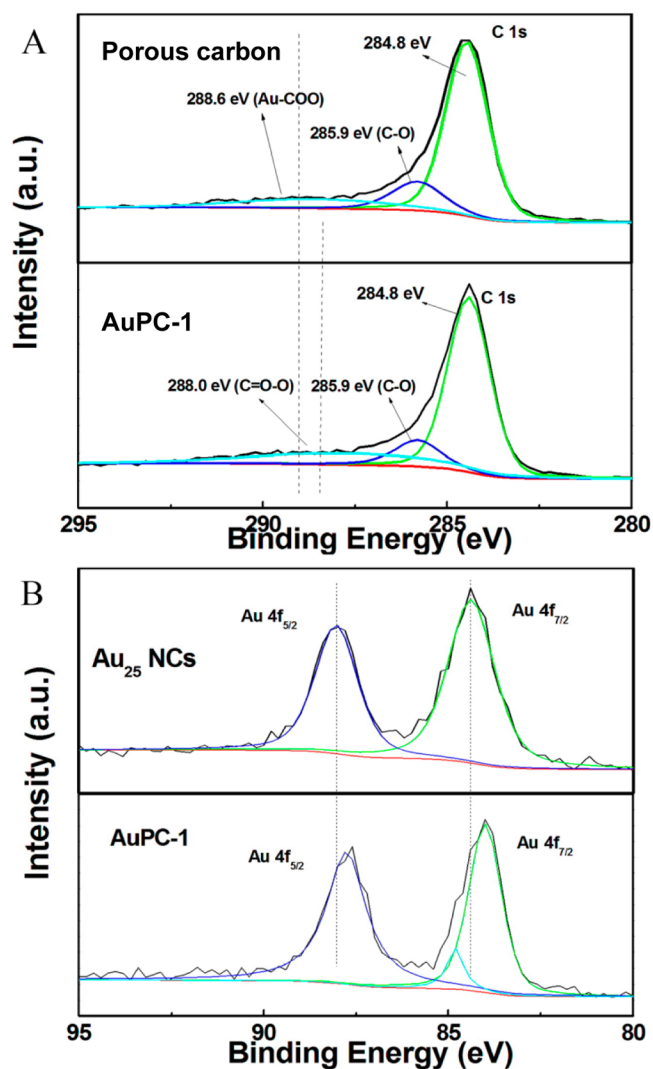
with the porous carbon alone except that the binding energy of carbonyl/carboxylic C was about 0.6 eV lower. This implies the formation of $Au-COO^-$ moieties in the AuPC hybrids.[34] This is consistent with the red-shift of the Au 4f electrons by 0.2−0.3 eV with AuPC-1 (87.8 and 84.0 eV) as compared with the original nanoclusters (88.0 and 84.4 eV) (Figure 3B). This suggests electron transfer from the carboxylic/carbonyl moieties to gold, and it is likely that the enhanced electron density on Au possessed an positive influence on the oxygen electroreduction activity (vide infra).

The electrochemical activity of the AuPC nanocomposites in alkaline media was then tested and compared. Experimentally, the glassy carbon electrode (GCE) surface was coated with a same amount of the hybrids for electrochemical tests. Figure 4A depicts the cyclic voltammetric (CV) measurements acquired with the AuPC-modified electrodes in a 0.1 M KOH solution with the potential scan rate of 10 mV s^{-1}. In the N_2-saturated KOH solution (black dash curves), no redox peak appeared within the potential range of 0.04 to 1.16 V. However, a well-defined voltammetric peak emerged in oxygen-saturated 0.1 M KOH solution, indicating obvious activity of AuPC in oxygen electroreduction. Yet the peak potentials (E_p) are clearly
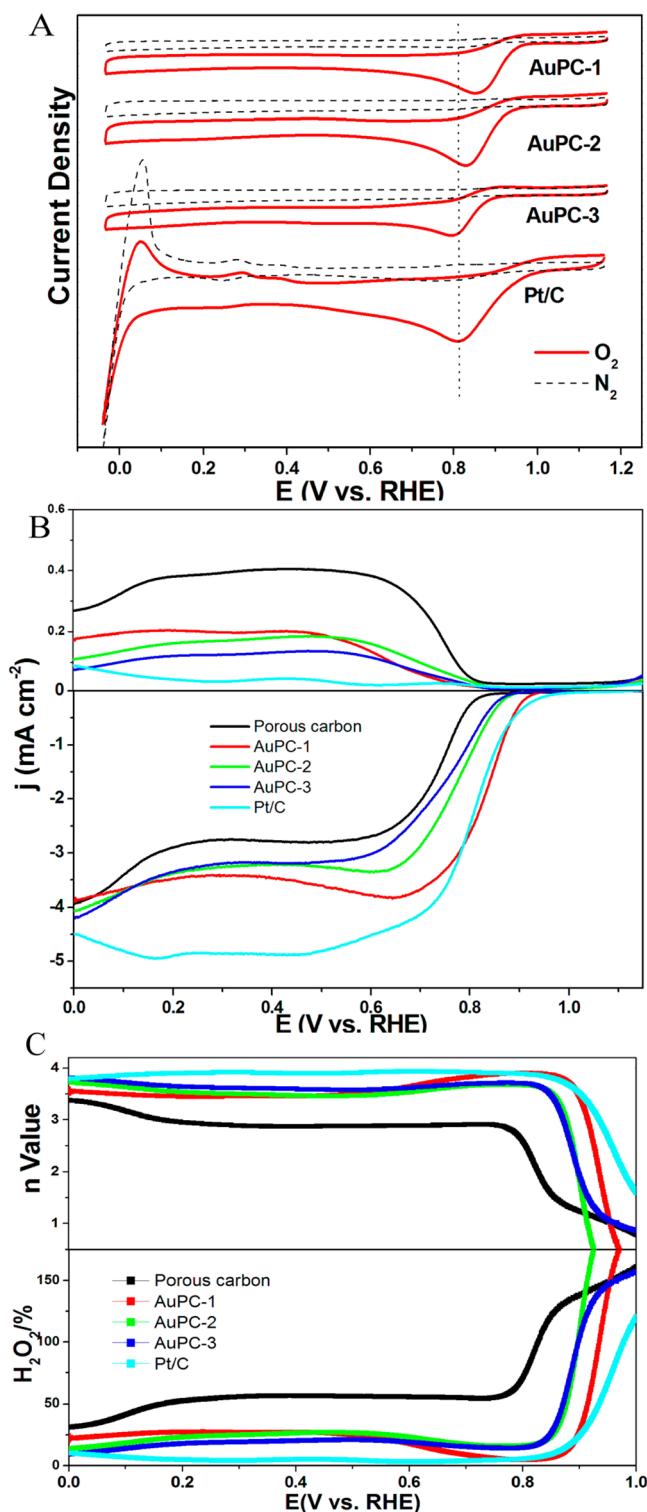
Figure 4. (A) CV curves of AuPC-1, AuPC-2, AuPC-3 nanocomposites, and commercial Pt/C catalysts recorded in nitrogen-saturated and oxygen-saturated 0.1 M KOH, and (B) The ORR polarization curves of porous carbon, AuPC-1, AuPC-2, AuPC-3 nanocomposites, and commercial Pt/C catalysts in O_2-saturated 0.1 M KOH with a rotation speed of 2500 rpm. (C) Variation of H_2O_2 yield and electron transfer number at various potentials.

different from sample to sample, at +0.86 V for AuPC-1, +0.83 V for AuPC-2, and +0.80 V for AuPC-3. Note that only +0.81 V was achieved for commercial Pt/C. Significant differences of

the peak current density (j_P) can also be seen at AuPC-1 (0.45 mA cm^{-2}), AuPC-2 (0.36 mA cm^{-2}), and AuPC-3 (0.33 mA cm^{-2}), and the value of commercial Pt/C is 0.57 mA cm^{-2}. The above results suggest that within the present experimental context, AuPC-1 emerged as the optimal oxygen electro-reduction catalyst, and the electrocatalytic capability was close to that of Pt/C.

RRDE measurements showed consistent results (Figure 4B). For instance, the onset potential (E_{onset}) of AuPC-1 is +0.95 V, whereas only +0.81 V for porous carbon, + 0.91 V for AuPC-2 and +0.89 V for AuPC-3. Additionally, one can see that at +0.45 V, AuPC-1 exhibited a much enhanced diffusion-limited current density of 3.61 mA cm^{-2} at 2500 rpm, in comparison with porous carbon (2.75 mA cm^{-2}), AuPC-2 (3.21 mA cm^{-2}), and AuPC-3 (3.16 mA cm^{-2}). Furthermore, E_{onset} was estimated to be +0.95 V for commercial 20 wt % Pt/C, along with a limiting current density of ca. 4.98 mA cm^{-2}. Taken together, these observations indicate that the ORR activity increases with the decreasing gold nanoparticle size, and the optimal performances were as good as that of Pt/C (Table 1).

Interestingly, the reduction current on AuPC-1 and AuPC-2 catalysts shows a maximum between +0.6 and +0.7 V (Figure 4B), followed by a slight decrease of current at more negative potentials. Such behaviors have been observed in previous reports.[35,36] The former might be assigned to the formation of HO_2^- on Au(111) and Au(100) facets, while the latter is probably attributed to the further reduction to OH^-.[35,36]

Control experiments with unsupported AuNCs further highlight the significance of the formation of AuPC hybrids in ORR, as depicted in Figures S7−S9 and listed in Table 1. It is obviously shown that for the three (AuPC) nanocomposites, the onset potentials were at least 200 mV more positive than those of unsupported AuNCs, and the current density at +0.45 V was also markedly higher by approximately 3.0 mA cm^{-2}. These observations showed that while the gold nanoparticles were somewhat larger, the formation of AuPC nanocomposites offered an effective strategy for the fabrication of highly efficient ORR electrocatalysts. This may be ascribed to the unique interactions between the Au NPs and the porous carbon support, as manifested in XPS measurements (Figure 3). Further contributions may arise from the porous carbon substrates (Figure S2) that facilitated the mass and electron transfer for ORR.

From the RRDE voltammograms, the number of electron transfer (n) and H_2O_2 percent yield may also be quantified by using the following equations:

$$n = \frac{4I_d}{I_d + \frac{I_r}{N}} \tag{1}$$

$$H_2O_2\% = \frac{\frac{200I_r}{N}}{\frac{I_r}{N} + I_d} \tag{2}$$

where I_d and I_r are the disk current and the ring current in RRDE voltammogrametric measurement, respectively. And N is the current collection efficiency (0.37). From Figure 4C, it can be seen that at potentials from +0.50 to +0.80 V, n was 2.61−2.89 for porous carbon, 3.60−3.92 for AuPC-1, 3.49−3.67 for AuPC-2, and 3.62−3.70 for AuPC-3, and the H_2O_2 yield was <23% for AuPC-1, AuPC-2, and AuPC-3 nanocomposites, slightly exceeded that of commercial Pt/C (~10%).

Table 1. Comparison of the ORR Activity of Different Samples Calculated by Voltammetric Measurements in 0.1 M KOH Solution

sample	E_P (V)[a]	j_P (mA cm^{-2})[a]	E_{onset} (V)[b]	$E_{1/2}$ (V)[b]	j (mA cm^{-2}) at +0.45 V[b]	ECSA (m^2 g^{-1})	specific activity at +0.80 V (mA cm^{-2})	mass activity at +0.80 V (A g^{-1})
AuPC-1	+0.86	0.45	+0.95	+0.83	3.61	32.02	0.612	25.50
AuPC-2	+0.83	0.36	+0.91	+0.78	3.21	30.13	0.195	8.13
AuPC-3	+0.80	0.33	+0.89	+0.75	3.16	27.27	0.160	6.67
Au$_{25}$(SC$_2$H$_4$Ph)$_{18}$	+0.54	0.19	+0.72	+0.57	0.63			
Au$_{38}$(SC$_2$H$_4$Ph)$_{24}$	+0.54	0.14	+0.71	+0.56	0.61			
Au$_{144}$(SC$_2$H$_4$Ph)$_{60}$	+0.50	0.10	+0.65	+0.54	0.35			
commercial Pt/C	+0.81	0.57	+0.95	+0.81	4.98	43.05	0.615	38.44

[a]E_P and j_P were determined from cyclic voltammograms (Figure 4A and Figure S7A). [b]E_{onset}, $E_{1/2}$, and j at 0.45 V were determined from rotating-disk voltammograms with a rotation speed of 2500 rpm (Figure 4B and Figure S7B).

Further insights may be obtained from the Tafel plots, which were constructed from RDE voltammograms acquired with different rotation speeds of 100−2500 rpm (Figure S10). Notably, the current density of three AuPC samples increased with the electrode rotation rates in RDE measurements, as manifested in the Koutecky−Levich plots within the kinetics/diffusion-mixed controlled region, where good linearity and consistent slopes suggested first-order reaction kinetics for oxygen reduction with regard to the oxygen concentration in the solution. As displayed in Figure 5A, the specific activity (j_k, normalized by the ECSA of the AuPC samples) increased with the decreasing of AuPC nanoparticle size. For instance, at +0.80 V, j_k increases in the order of 0.160 mA cm^{-2} (AuPC-3) < 0.195 mA cm^{-2} (AuPC-2) < 0.612 mA cm^{-2} (AuPC-1) < 0.615 mA cm^{-2} (commercial Pt/C). Note that the specific activity

value of AuPC-1 is almost identical to that of Pt/C. A similar trend can be observed with the mass activity (kinetic currents normalized to the metal mass), of which the order is 6.67 A g^{-1} (AuPC-3) < 8.13 A g^{-1} (AuPC-2) < 25.50 A g^{-1} (AuPC-1) < 38.44 A g^{-1} (commercial Pt/C). The values are also listed in Table 1. Additionally, similar features of the Tafel plots were obtained for the various catalysts. The Tafel plots actually displayed two clear linear regions at low and high over-potentials, which has been recorded rather extensively in previous studies.[3−6] In the low overpotential range (where ET kinetics was more likely the limiting factor in ORR), the slopes were found at 62.6 mV dec^{-1} for AuPC-1, 59.5 mV dec^{-1} for AuPC-2, 57.8 mV dec^{-1} for AuPC-3, and 78.5 mV dec^{-1} for Pt/C. The Tafel slopes were all around 60 mV dec^{-1}, indicating that the rate-determining step in the electrocatalytic reduction of O$_2$ might be a pseudo two-electron reaction.[26] However, at the potential below +0.85 V, the slopes were 123.1 mV dec^{-1} for AuPC-1, 119.1 mV dec^{-1} for AuPC-2, 118.3 mV dec^{-1} for AuPC-3, and 123.8 mV dec^{-1} for Pt/C, suggesting that the reaction rate was probably determined by the first electron transfer to oxygen molecules.[3−6]

The following factors mainly contributed to the apparent ORR activity of the AuPC samples: First of all, the small-sized Au particles are beneficial for the activation of molecular oxygen, as the low-coordination surface Au atoms can significantly decrease the activation energy of chemisorption of oxygen molecule,[23,37,38] which facilitates the 4-electron transfer and leads to a positive onset potential; Second, the complete removal of the thiolate ligands promotes interfacial charge transfer from carbon to gold during ORR,[22,39,40] as evidenced from the XPS measurements (Figure 3); At last, the integration of porous carbon and Au offers a synergetic platform for improved ORR activity, as porous carbon acts not only as a support and but also had an inevitable influence on metal−support interactions.[15,41−43]

Finally, the durability and stability in alkaline media of these nanocomposite catalysts were investigated by chronoamperometric measurements. From Figure 5B, the cathodic currents of AuPC-1, AuPC-2, and AuPC-3 exhibited a loss of 19.2%, 15.6%, and 22.7% after continuous operation for over 8 h, whereas Pt/C displayed a 35% loss. The remarkable long-term stability might be attributed to the porous carbon support that prevented the aggregation of AuNCs while maintaining efficient electron transport for ORR. In fact, the electrochemical performance of AuPC-1 was highly reproducible even after three repeated uses (Figure S11).
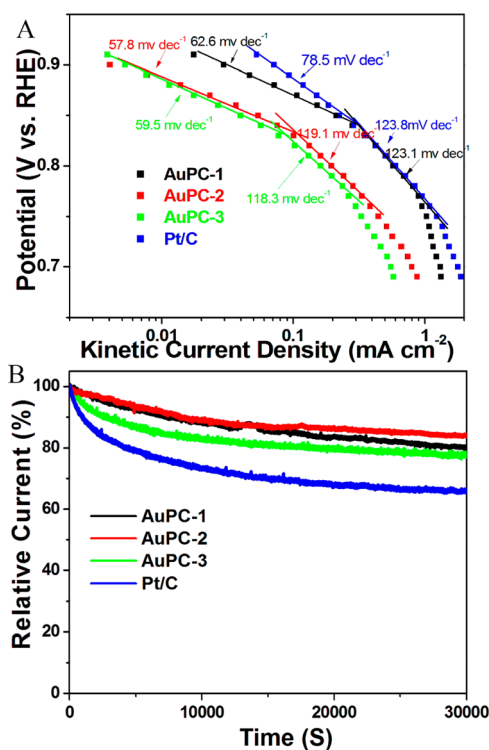

Figure 5. (A) Tafel plots of AuPC-1, AuPC-2, AuPC-3, and commercial Pt/C catalysts. Data obtained from linear fitting of the K−L plots in Figure S10. (B) Chronoamperometric profiles at the AuPC-1, AuPC-2, AuPC-3, and commercial Pt/C electrodes in the oxygen-saturated 0.1 M KOH solution with a rotation speed of 900 rpm at constant overpotential of +0.5 V (vs RHE) for 30 000 s.

CONCLUSIONS

Porous carbon-supported gold nanoparticles were prepared by using molecular gold nanoclusters as precursors that were embedded within porous carbon matrices. Obvious electrocatalytic activity toward ORR was observed with the nanocomposites in alkaline media, where the performance varied with the nanoparticles size. Among the series of samples tested, the nanocomposite prepared with Au_{25} nanoclusters demonstrated the best electrocatalytic activity, evidenced by an onset potential at +0.95 V vs RHE, the electron transfer number of 3.60−3.92 within the potential range of +0.50 to +0.80 V, and remarkable long-term stability. The performance is competitive with that of commercial 20 wt % Pt/C. The results highlight the feasibility of using porous carbon-supported gold nanoparticles as high-efficiency ORR catalysts.

ASSOCIATED CONTENT

Ⓢ Supporting Information

The Supporting Information is available free of charge on the ACS Publications website at DOI: 10.1021/acsami.6b02223.

> Experimental details of the preparation of AuNCs and porous carbon, UV−visible spectra, TEM, TGA of AuNCs, XPS of porous carbon, AuNCs, AuPCs, and additional electrochemical results of the samples (PDF)

AUTHOR INFORMATION

Corresponding Authors

*E-mails: zhht@scut.edu.cn (Z.H.T.).
*E-mails: shaowei@ucsc.edu (S.W.C.).

Author Contributions

The manuscript was written through contributions of all authors. All authors have given approval to the final version of the manuscript.

Notes

The authors declare no competing financial interest.

ACKNOWLEDGMENTS

REFERENCES

(1) Borup, R.; Meyers, J.; Pivovar, B.; Kim, Y. S.; Mukundan, R.; Garland, N.; Myers, D.; Wilson, M.; Garzon, F.; Wood, D.; Zelenay, P.; More, K.; Stroh, K.; Zawodzinski, T.; Boncella, J.; McGrath, J. E.; Inaba, M.; Miyatake, K.; Hori, M.; Ota, K.; Ogumi, Z.; Miyata, S.; Nishikata, A.; Siroma, Z.; Uchimoto, Y.; Yasuda, K.; Kimijima, K.-i.; Iwashita, N. Scientific Aspects of Polymer Electrolyte Fuel Cell Durability and Degradation. *Chem. Rev.* **2007**, *107*, 3904−3951.

(2) Debe, M. K. Electrocatalyst Approaches and Challenges for Automotive Fuel Cells. *Nature* **2012**, *486*, 43−51.

(3) Liu, M.; Zhang, R.; Chen, W. Graphene-Supported Nanoelectrocatalysts for Fuel Cells: Synthesis, Properties, and Applications. *Chem. Rev.* **2014**, *114*, 5117−5160.

(4) Guo, S.; Zhang, S.; Sun, S. Tuning Nanoparticle Catalysis for the Oxygen Reduction Reaction. *Angew. Chem., Int. Ed.* **2013**, *52*, 8526−8544.

(5) Cui, C.-H.; Yu, S.-H. Engineering Interface and Surface of Noble Metal Nanoparticle Nanotubes toward Enhanced Catalytic Activity for Fuel Cell Applications. *Acc. Chem. Res.* **2013**, *46*, 1427−1437.

(6) He, G.; Song, Y.; Liu, K.; Walter, A.; Chen, S.; Chen, S. Oxygen Reduction Catalyzed by Platinum Nanoparticles Supported on Graphene Quantum Dots. *ACS Catal.* **2013**, *3*, 831−838.

(7) Liang, J.; Du, X.; Gibson, C.; Du, X. W.; Qiao, S. Z. N-Doped Graphene Natively Grown on Hierarchical Ordered Porous Carbon for Enhanced Oxygen Reduction. *Adv. Mater.* **2013**, *25*, 6226−6231.

(8) Ding, W.; Li, L.; Xiong, K.; Wang, Y.; Li, W.; Nie, Y.; Chen, S.; Qi, X.; Wei, Z. Shape Fixing via Salt Recrystallization: A Morphology-Controlled Approach To Convert Nanostructured Polymer to Carbon Nanomaterial as a Highly Active Catalyst for Oxygen Reduction Reaction. *J. Am. Chem. Soc.* **2015**, *137*, 5414−5420.

(9) Niu, W.; Li, L.; Liu, X.; Wang, N.; Liu, J.; Zhou, W.; Tang, Z.; Chen, S. Mesoporous N-Doped Carbons Prepared with Thermally Removable Nanoparticle Templates: An Efficient Electrocatalyst for Oxygen Reduction Reaction. *J. Am. Chem. Soc.* **2015**, *137*, 5555−5562.

(10) Wang, Q.; Zhou, Z.-Y.; Lai, Y.-J.; You, Y.; Liu, J.-G.; Wu, X.-L.; Terefe, E.; Chen, C.; Song, L.; Rauf, M.; Tian, N.; Sun, S.-G. Phenylenediamine-Based FeNx/C Catalyst with High Activity for Oxygen Reduction in Acid Medium and Its Active-Site Probing. *J. Am. Chem. Soc.* **2014**, *136*, 10882−10885.

(11) Chung, D. Y.; Jun, S. W.; Yoon, G.; Kwon, S. G.; Shin, D. Y.; Seo, P.; Yoo, J. M.; Shin, H.; Chung, Y.-H.; Kim, H.; Mun, B. S.; Lee, K.-S.; Lee, N.-S.; Yoo, S. J.; Lim, D.-H.; Kang, K.; Sung, Y.-E.; Hyeon, T. Highly Durable and Active PtFe Nanocatalyst for Electrochemical Oxygen Reduction Reaction. *J. Am. Chem. Soc.* **2015**, *137*, 15478−15485.

(12) Shao, M.; Peles, A.; Shoemaker, K. Electrocatalysis on Platinum Nanoparticles: Particle Size Effect on Oxygen Reduction Reaction Activity. *Nano Lett.* **2011**, *11*, 3714−3719.

(13) Erikson, H.; Jürmann, G.; Sarapuu, A.; Potter, R. J.; Tammeveski, K. Electroreduction of Oxygen on Carbon-Supported Gold Catalysts. *Electrochim. Acta* **2009**, *54*, 7483−7489.

(14) Erikson, H.; Sarapuu, A.; Tammeveski, K.; Solla-Gullón, J.; Feliu, J. M. Shape-Dependent Electrocatalysis: Oxygen Reduction on Carbon-Supported Gold Nanoparticles. *ChemElectroChem* **2014**, *1*, 1338−1347.

(15) Yin, H.; Tang, H.; Wang, D.; Gao, Y.; Tang, Z. Facile Synthesis of Surfactant-Free Au Cluster/Graphene Hybrids for High-Performance Oxygen Reduction Reaction. *ACS Nano* **2012**, *6*, 8288−8297.

(16) Uosaki, K.; Elumalai, G.; Noguchi, H.; Masuda, T.; Lyalin, A.; Nakayama, A.; Taketsugu, T. Boron Nitride Nanosheet on Gold as an Electrocatalyst for Oxygen Reduction Reaction: Theoretical Suggestion and Experimental Proof. *J. Am. Chem. Soc.* **2014**, *136*, 6542−6545.

(17) Morozan, A.; Donck, S.; Artero, V.; Gravel, E.; Doris, E. Carbon Nanotubes-Gold Nanohybrid as Potent Electrocatalyst for Oxygen Reduction in Alkaline Media. *Nanoscale* **2015**, *7*, 17274−17277.

(18) Bogdanović, U.; Pašti, I.; Ćirić-Marjanović, G.; Mitrić, M.; Ahrenkiel, S. P.; Vodnik, V. Interfacial Synthesis of Gold−Polyaniline Nanocomposite and Its Electrocatalytic Application. *ACS Appl. Mater. Interfaces* **2015**, *7*, 28393−28403.

(19) Zhang, G.-R.; Xu, B.-Q. Nano-size Effect of Au Catalyst for Electrochemical Reduction of Oxygen in Alkaline Electrolyte. *Chin. J. Catal.* **2013**, *34*, 942−948.

(20) Tang, W.; Lin, H.; Kleiman-Shwarsctein, A.; Stucky, G. D.; McFarland, E. W. Size-Dependent Activity of Gold Nanoparticles for Oxygen Electroreduction in Alkaline Electrolyte. *J. Phys. Chem. C* **2008**, *112*, 10515−10519.

(21) Inasaki, T.; Kobayashi, S. Particle Size Effects of Gold on the Kinetics of the Oxygen Reduction at Chemically Prepared Au/C Catalysts. *Electrochim. Acta* **2009**, *54*, 4893−4897.

(22) Lee, Y.; Loew, A.; Sun, S. Surface- and Structure-Dependent Catalytic Activity of Au Nanoparticles for Oxygen Reduction Reaction. *Chem. Mater.* **2010**, *22*, 755−761.

(23) Chen, W.; Chen, S. Oxygen Electroreduction Catalyzed by Gold Nanoclusters: Strong Core Size Effects. *Angew. Chem., Int. Ed.* **2009**, *48*, 4386−4389.

(24) Elliott, E. W.; Glover, R. D.; Hutchison, J. E. Removal of Thiol Ligands from Surface-Confined Nanoparticles without Particle Growth or Desorption. *ACS Nano* **2015**, *9*, 3050–3059.

(25) Goncalves, G.; Marques, P. A. A. P.; Granadeiro, C. M.; Nogueira, H. I. S.; Singh, M. K.; Grácio, J. Surface Modification of Graphene Nanosheets with Gold Nanoparticles: The Role of Oxygen Moieties at Graphene Surface on Gold Nucleation and Growth. *Chem. Mater.* **2009**, *21*, 4796–4802.

(26) Lin, C.; Song, Y.; Cao, L.; Chen, S. Oxygen Reduction Catalyzed by Au−TiO2 Nanocomposites in Alkaline Media. *ACS Appl. Mater. Interfaces* **2013**, *5*, 13305–13311.

(27) Jin, C.; Cao, X.; Lu, F.; Yang, Z.; Yang, R. Facile Synthesis of Gold-Nanoparticle-Decorated Gd0.3Ce0.7O1.9 Nanotubes with Enhanced Catalytic Activity for Oxygen Reduction Reaction. *ACS Appl. Mater. Interfaces* **2014**, *6*, 847–853.

(28) Jun, S.; Joo, S. H.; Ryoo, R.; Kruk, M.; Jaroniec, M.; Liu, Z.; Ohsuna, T.; Terasaki, O. Synthesis of New, Nanoporous Carbon with Hexagonally Ordered Mesostructure. *J. Am. Chem. Soc.* **2000**, *122*, 10712–10713.

(29) Yao, C.; Chen, J.; Li, M.-B.; Liu, L.; Yang, J.; Wu, Z. Adding Two Active Silver Atoms on Au25 Nanoparticle. *Nano Lett.* **2015**, *15*, 1281–1287.

(30) Qian, H.; Zhu, Y.; Jin, R. Size-Focusing Synthesis, Optical and Electrochemical Properties of Monodisperse Au(38) (SC(2)H(4)Ph)(24) Nanoclusters. *ACS Nano* **2009**, *3*, 3795–3803.

(31) Qian, H.; Jin, R. Controlling Nanoparticles with Atomic Precision: The Case of Au(144) (SCH(2)CH(2)Ph)(60). *Nano Lett.* **2009**, *9*, 4083–4087.

(32) Murray, R. W. Nanoelectrochemistry: Metal Nanoparticles, Nanoelectrodes, and Nanopores. *Chem. Rev.* **2008**, *108*, 2688–2720.

(33) Varnavski, O.; Ramakrishna, G.; Kim, J.; Lee, D.; Goodson, T. Critical Size for the Observation of Quantum Confinement in Optically Excited Gold Clusters. *J. Am. Chem. Soc.* **2010**, *132*, 16–17.

(34) Park, J.-W.; Shumaker-Parry, J. S. Strong Resistance of Citrate Anions on Metal Nanoparticles to Desorption under Thiol Functionalization. *ACS Nano* **2015**, *9*, 1665–1682.

(35) Sarapuu, A.; Nurmik, M.; Mändar, H.; Rosental, A.; Laaksonen, T.; Kontturi, K.; Schiffrin, D. J.; Tammeveski, K. Electrochemical Reduction of Oxygen on Nanostructured Gold Electrodes. *J. Electroanal. Chem.* **2008**, *612*, 78–86.

(36) Adžić, R. R.; Strbac, S.; Anastasijević, N. Electrocatalysis of Oxygen on Single Crystal Gold Electrodes. *Mater. Chem. Phys.* **1989**, *22*, 349–375.

(37) Pal, R.; Wang, L.-M.; Pei, Y.; Wang, L.-S.; Zeng, X. C. Unraveling the Mechanisms of O2 Activation by Size-Selected Gold Clusters: Transition from Superoxo to Peroxo Chemisorption. *J. Am. Chem. Soc.* **2012**, *134*, 9438–9445.

(38) Jeyabharathi, C.; Senthil Kumar, S.; Kiruthika, G. V. M; Phani, K. L. N. Aqueous CTAB-Assisted Electrodeposition of Gold Atomic Clusters and Their Oxygen Reduction Electrocatalytic Activity in Acid Solutions. *Angew. Chem., Int. Ed.* **2010**, *49*, 2925–2928.

(39) Li, D.; Wang, C.; Tripkovic, D.; Sun, S.; Markovic, N. M.; Stamenkovic, V. R. Surfactant Removal for Colloidal Nanoparticles from Solution Synthesis: The Effect on Catalytic Performance. *ACS Catal.* **2012**, *2*, 1358–1362.

(40) Chen, W.; Ny, D.; Chen, S. SnO2−Au Hybrid Nanoparticles as Effective Catalysts for Oxygen Electroreduction in Alkaline Media. *J. Power Sources* **2010**, *195*, 412–418.

(41) Slanac, D. A.; Lie, A.; Paulson, J. A.; Stevenson, K. J.; Johnston, K. P. Bifunctional Catalysts for Alkaline Oxygen Reduction Reaction via Promotion of Ligand and Ensemble Effects at Ag/MnOx Nanodomains. *J. Phys. Chem. C* **2012**, *116*, 11032–11039.

(42) Zhang, C.; Xu, L.; Shan, N.; Sun, T.; Chen, J.; Yan, Y. Enhanced Electrocatalytic Activity and Durability of Pt Particles Supported on Ordered Mesoporous Carbon Spheres. *ACS Catal.* **2014**, *4*, 1926–1930.

(43) Ding, J.; Chan, K.-Y.; Ren, J.; Xiao, F.-S. Platinum and Platinum−Ruthenium Nanoparticles Supported on Ordered Meso- porous Carbon and Their Electrocatalytic Performance for Fuel Cell Reactions. *Electrochim. Acta* **2005**, *50*, 3131–3141.

Porous Carbon-Supported Gold Nanoparticles for Oxygen Reduction Reaction: Effects of Nanoparticle Size

Likai Wang,[a] Zhenghua Tang,*[a,b] Wei Yan,[a] Hongyu Yang,[a] Qiannan Wang,[a] and Shaowei Chen*[a,c]

*a*New Energy Research Institute, School of Environment and Energy, South China University of Technology, Guangzhou Higher Education Mega Centre, Guangzhou, 510006, P. R. China. *Email:* zhht@scut.edu.cn.
*b*Guangdong Provincial Key Laboratory of Atmospheric Environment and Pollution Control, South China University of Technology, Guangzhou Higher Education Mega Centre, Guangzhou, 510006, P. R. China
*c*Department of Chemistry and Biochemistry, University of California, 1156 High Street, Santa Cruz, California 95064, United States. Email: shaowei@ucsc.edu

Preparation of porous carbons

Porous carbons were prepared by following a previous synthetic method.[1] Firstly, an aqueous solution was prepared by dissolving 1.25 g of sucrose and 0.14 g of H_2SO_4 in 5 mL of H_2O in a 50 mL Telfon-lined autoclave, and 1 g of SBA-15 amorphous silica was then added into the above aqueous solution. The mixture was under magnetic stirring for 2 h at room temperature, followed by heating at 100 °C for 6 h in an oven and at 160 °C for another 6 h. The precursor turned dark brown during the heating treatment in the oven. Secondly, the resultant precursor was again heated following the above procedure after the addition of 0.8 g sucrose, 0.09 g H_2SO_4 and 5 g H_2O. Finally, the obtained precursor underwent pyrolysis at 900 °C for 5 h under a N_2 flow, affording the preparation of carbon-silica composites, which were immersed in a 10 wt% HF solution for 24 h to remove the silica template, affording porous carbon which displayed ordered trenches of *ca.* 10 nm in diameter and several microns in length.[2]

Synthesis of $Au_{25}(SC_2H_4Ph)_{18}$

Au_{25} nanoclusters were prepared by adopting a previously reported approach.[3] Briefly, 1 mmol $HAuCl_4 \cdot 4H_2O$ and 1 mmol TOAB were co-dissolved in 30 mL THF in a 100 mL of round-bottom flask, and the resulting solution was cooled to 0 °C in an ice bath over a period of 30 min. 6 mmol of $PhCH_2CH_2SH$ was slowly added to the flask; the speed of stirring was turned to be very low (60 rpm) until the red color solution turned colorless in ~3 h. Then, the stirring speed was increased to 1100 rpm, and an aqueous solution of $NaBH_4$ (10 mmol freshly dissolved with 5 mL ice-cold nanopure water) was rapidly added all at once. The reaction was under vigorous stirring for 12 h. After removal of some precipitates (by-products), the solution was concentrated by rotary evaporation. Then cold water was added, and the precipitates were collected and thoroughly washed with methanol for five times to remove excess thiol. The as-obtained solids were the $Au_{25}(SC_2H_4Ph)_{18}$ nanoclusters.

Synthesis of $Au_{38}(SC_2H_4Ph)_{24}$

Au_{38} nanoclusters were prepared according to a previously reported method.[4] Firstly, 196.9 mg of $HAuCl_4 \cdot 3H_2O$ and 614 mg of glutathione (GSH) were vigorously stirred at room temperature for 30 min in 20 mL acetone, then the mixture was cooled to ~0 °C in an ice bath over a period of 20 min. Subsequently, a freshly prepared aqueous solution of $NaBH_4$ (5 mmol, dissolved with 6 mL ice-cold nanopure water) was

rapidly added into the suspension under vigorous stirring. After 20 min, black $Au_n(SG)_m$ nanoparticles were precipitated out of the solution. The clear acetone supernatant was removed, and the polydisperse $Au_n(SG)_m$ nanoparticles were dissolved with 7 mL nanopure water, and mixed with 0.4 mL ethanol, 2 mL toluene and 2 mL PhC_2H_4SH in a 25 mL of round-bottom flask under vigorous stirring at ambient temperature for 1 h. Then the biphase solution was heated to 80 °C and kept at this temperature for ~40 h. The organic phase was washed with methanol for five times to remove excess thiol, and $Au_{38}(SC_2H_4Ph)_{24}$ nanoclusters were separated by extraction with dichloromethane.

Synthesis of $Au_{144}(SC_2H_4Ph)_{60}$

Au_{144} nanoclusters were prepared in reference to a previous method.[5] Typically, 196.9 mg of $HAuCl_4 \cdot 3H_2O$ was dissolved in 6 mL nanopure water, and 314.6 mg of TOAB was dissolved in 10 mL toluene. These two solutions were mixed in a 25 mL of round-bottom flask under vigorous stirring at room temperature for 30 min. The clear aqueous phase was removed with a separatory funnel. The toluene solution containing Au(III) was cooled to ~0 °C in an ice bath over a period of 30 min. Then, 0.206 mL of $PhCH_2CH_2SH$ was added under vigorous stirring. The deep red solution turned colorless after ~2 h. An aqueous solution of $NaBH_4$ (5 mmol, dissolved in 6 mL ice-cold nanopure water) was rapidly added to the flask all at once under vigorous stirring. The reaction was allowed to proceed for ~24 h. Then, the aqueous phase was discarded and the black toluene phase was dried by rotary evaporation. The Au nanoparticles were separated by ethanol from TOAB and other side products. Then, excess $PhCH_2CH_2SH$ was used to etch the as-prepared Au nanoparticles. Generally, 80 mg Au nanoparticles were dissolved with 4 mL toluene, and 2 mL $PhCH_2CH_2SH$ was added to the solution. The mixture solution was heated at 80 °C for 24 h under constant stirring. After that, 80 mL methanol was added to the solution to precipitate Au nanoparticles. Only Au_{144} nanoclusters and $Au(I)-SCH_2CH_2Ph$ existed in the black precipitation. Au_{144} nanoclusters were extracted with dichloromethane as the final product
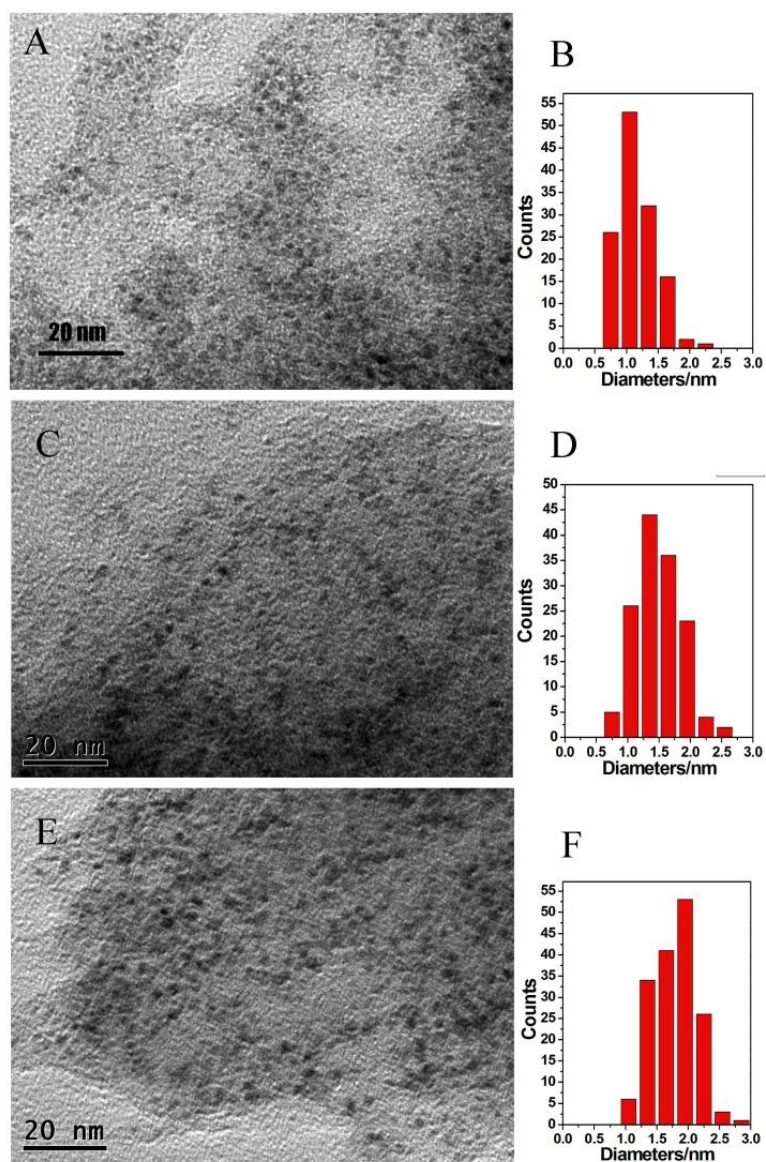
Figure S1. Representative TEM images of (A) $Au_{25}(SC_2H_4Ph)_{18,}$ (C) $Au_{38}(SC_2H_4Ph)_{24}$ and (E) $Au_{144}(SC_2H_4Ph)_{60}$ nanoclusters, with their corresponding core size histograms in panels (B), (D) and (F). The average core diameters were estimated to be 1.10 ± 0.30 nm, 1.20 ± 0.35 nm and 1.60 ± 0.50 nm, respectively.
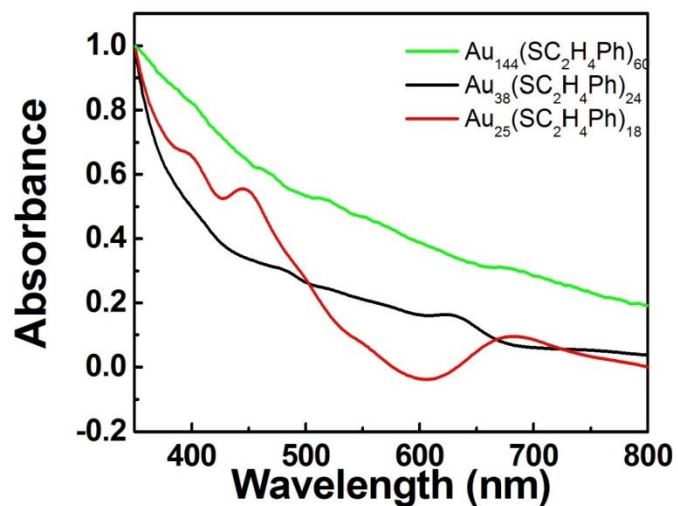
Figure S2. UV-visible absorption spectra of $Au_{25}(SC_2H_4Ph)_{18}$, $Au_{38}(SC_2H_4Ph)_{24}$ and $Au_{144}(SC_2H_4Ph)_{60}$. $Au_{25}(SC_2H_4Ph)_{18}$ nanoclusters showed distinct peaks at 400, 445, and 680 nm. $Au_{38}(SC_2H_4Ph)_{24}$ nanoclusters showed prominent peaks at 485 and 620 nm. $Au_{144}(SC_2H_4Ph)_{60}$ nanoclusters showed distinct bands at 510 and 700 nm.
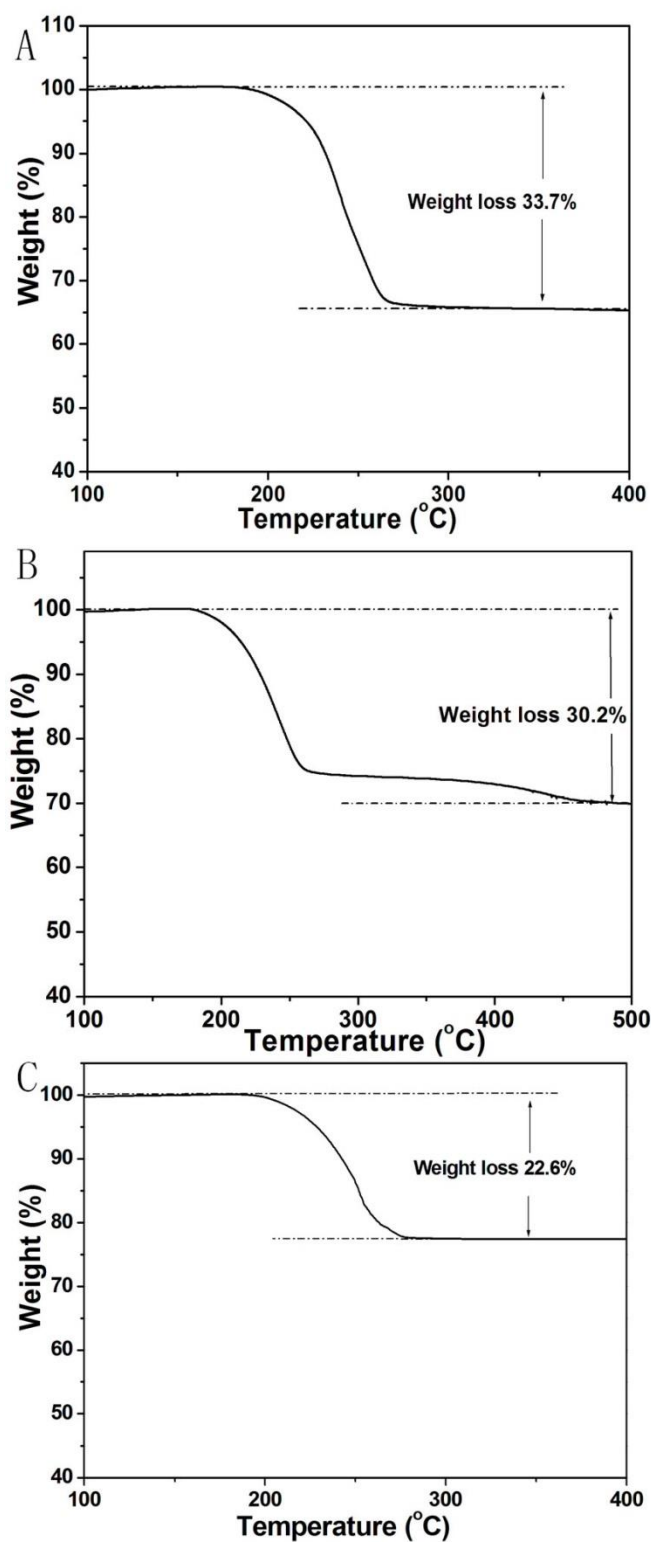
Figure S3. TGA curves of (A) $Au_{25}(SC_2H_4Ph)_{18,}$ (B) $Au_{38}(SC_2H_4Ph)_{24}$ and (C) $Au_{144}(SC_2H_4Ph)_{60}$ nanoclusters, where the organic components were estimated to account for about 33.7%, 30.2%, and 22.6% in the nanoparticles, in good agreement with the calculated values of 33.3%, 30.5%, 22.5%, respectively.
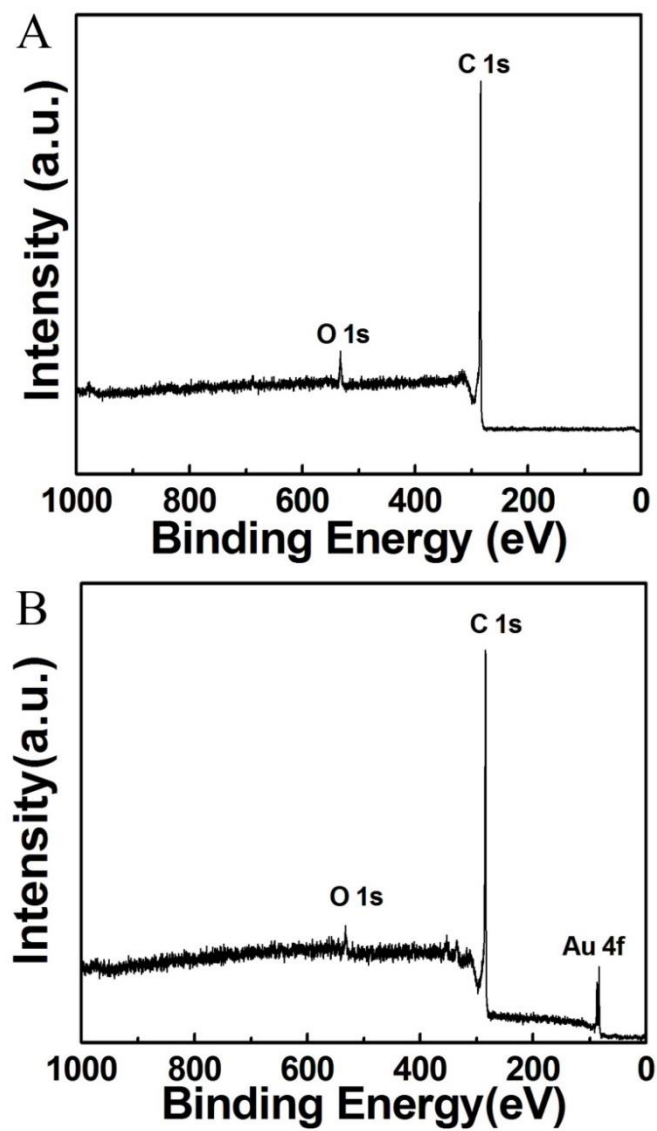
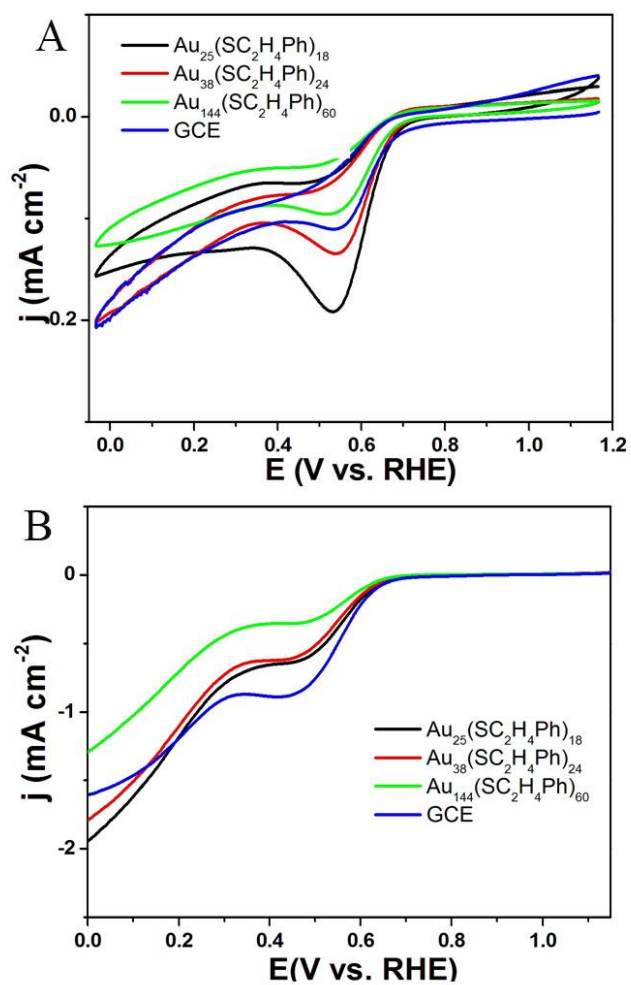**Figure S4.** XPS survey spectra of (A) porous carbon and (B) AuPC-1. In panel (B), based on the integrated peak areas, the gold loading was estimated to be 0.8 atom%.

Figure S5. (A) Cyclic voltammograms of GCE, $Au_{25}(SC_2H_4Ph)_{18}$, $Au_{38}(SC_2H_4Ph)_{24}$ and $Au_{144}(SC_2H_4Ph)_{60}$ in 0.1 M KOH solution saturated with oxygen at a scan rate of 10 mV/s. (B) RDE voltammograms of GCE, $Au_{25}(SC_2H_4Ph)_{18}$, $Au_{38}(SC_2H_4Ph)_{24}$ and $Au_{144}(SC_2H_4Ph)_{60}$ in 0.1 M KOH solution saturated with oxygen at the rotation rate of 2500 rpm.
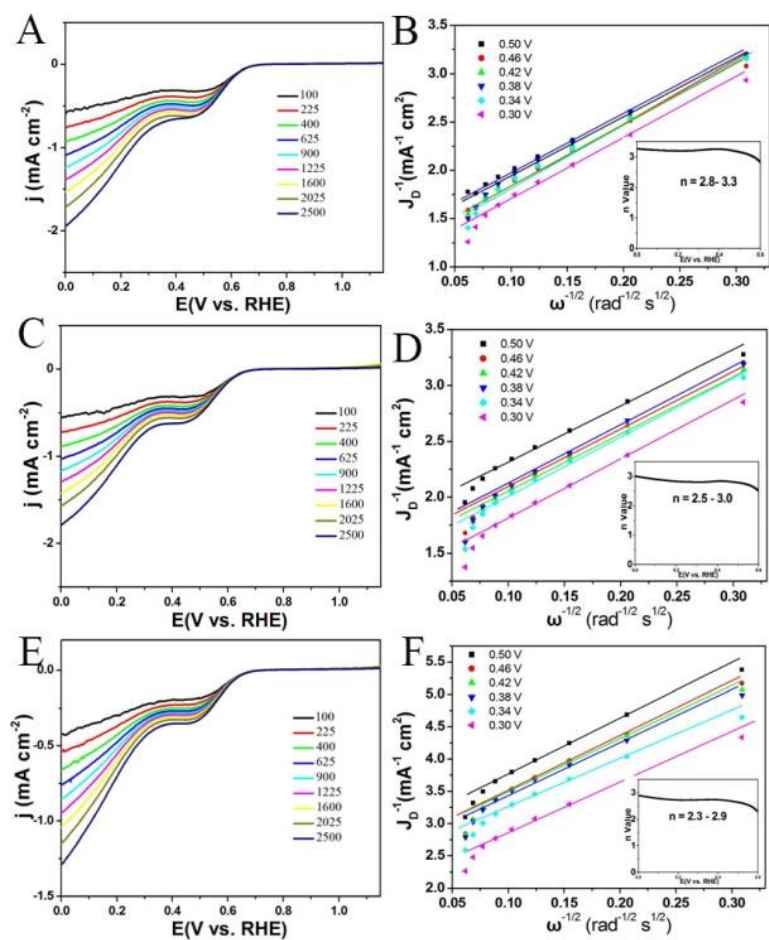
Figure S6. RDE voltammograms and corresponding Koutecky–Levich plots (j^{-1} versus $\omega^{-1/2}$) of different catalysts in O_2-saturated 0.1 M KOH with a sweep rate of 10 mV s^{-1} at different rotation rates: (A and B) $Au_{25}(SC_2H_4Ph)_{18}$, (C and D) $Au_{38}(SC_2H_4Ph)_{24}$ and (E and F) $Au_{144}(SC_2H_4Ph)_{60}$.
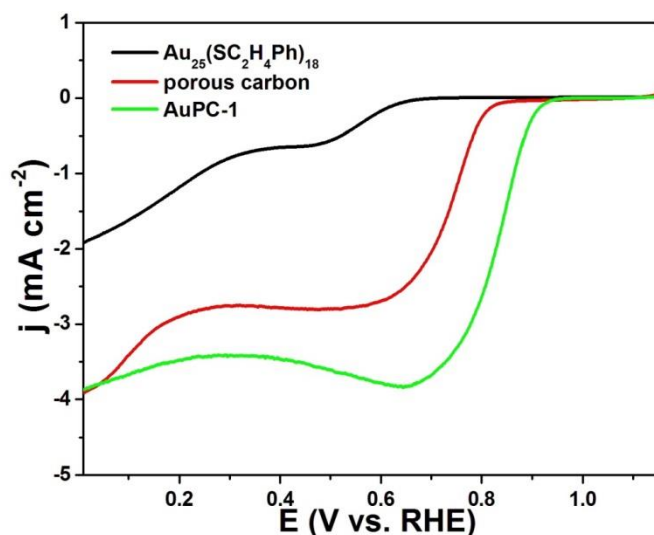
Figure S7. LSV curves for $Au_{25}(SC_2H_4Ph)_{18}$, porous carbon and AuPC-1 in 0.1 M KOH solution saturated with oxygen at the rotation rates of 2500 rpm.
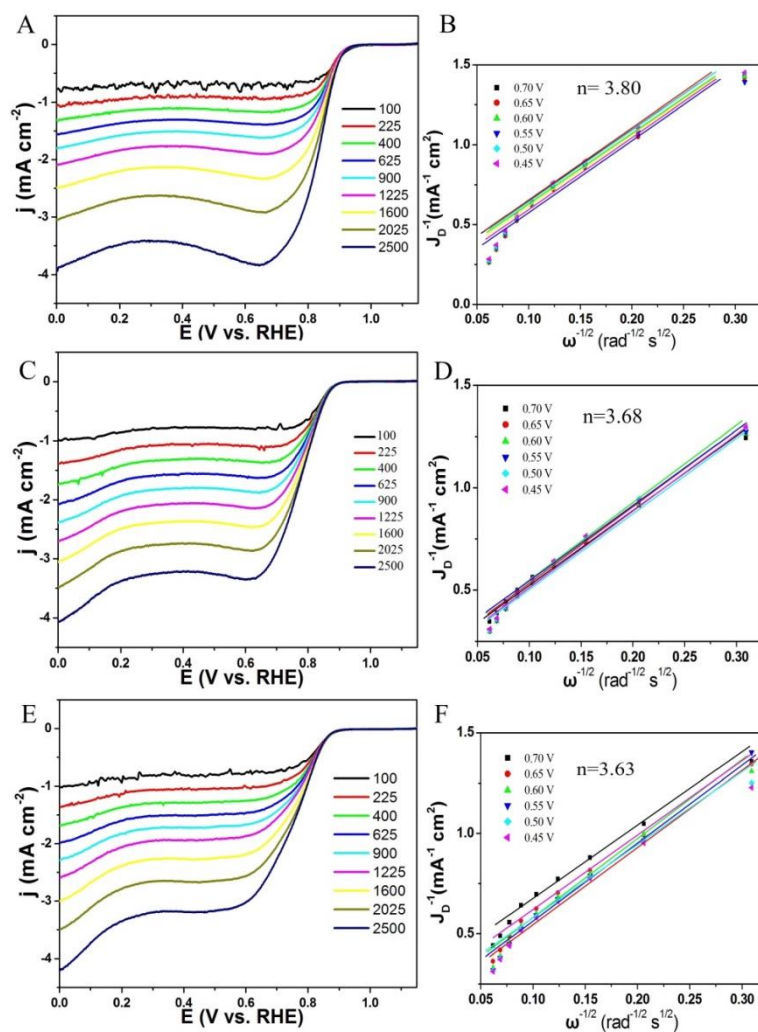
Figure S8. RDE voltammograms and corresponding Koutecky–Levich plots (j^{-1} versus $\omega^{-1/2}$) of different catalysts in O_2-saturated 0.1 M KOH with a sweep rate of 10 mV s^{-1} at different rotation rates: (A and B) AuPC-1, (C and D) AuPC-2, (E and F) AuPC-3.
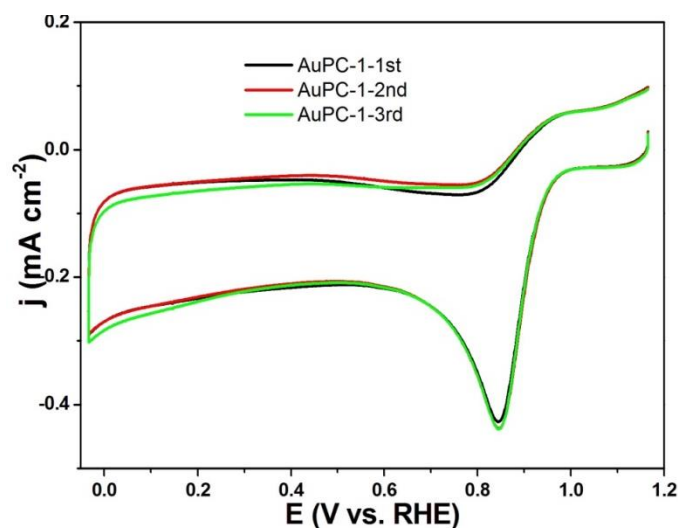
Figure S9. Cyclic voltammeograms of AuPC-1 in 0.1 M KOH solution after three repeated uses for ORR.

References

(1) Jun, S.; Joo, S. H.; Ryoo, R.; Kruk, M.; Jaroniec, M.; Liu, Z.; Ohsuna, T.; Terasaki, O. Synthesis of New, Nanoporous Carbon with Hexagonally Ordered Mesostructure. *J. Am. Chem. Soc.* **2000**, *122*, 10712-10713.

(2) Wang, L. K.; Tang, Z. H.; Liu, X. J.; Niu, W. H.; Zhou, K.; Yang, H. Y.; Zhou, W. J.; Li, L. G.; Chen, S. W. Ordered mesoporous carbons-supported gold nanoparticles as highly efficient electrocatalysts for oxygen reduction reaction. *RSC Adv.* **2015**, *5*, 103421-103427.

(3) Yao, C.; Chen, J.; Li, M. B.; Liu, L.; Yang, J.; Wu, Z. Adding Two Active Silver Atoms on Au Nanoparticle. *Nano Lett.* **2015**, *15*, 1281-1287.

(4) Qian, H.; Zhu, Y.; Jin, R. Size-Focusing Synthesis, Optical and Electrochemical Properties of Monodisperse Au38(SC2H4Ph)24 Nanoclusters. *ACS Nano* **2009**, *3*, 3795-3803.

(5) Qian, H.; Jin, R. Controlling Nanoparticles with Atomic Precision: The Case of Au144(SCH2CH2Ph)60. *Nano Lett.* **2009**, *9*, 4083-4087.